Flight-Test Evaluation of Engine Power Effects on Lift and Drag

T. R. Yechout*
United States Air Force Academy, Colorado Springs, Colorado
and
W. G. Schweikhard† and K. B. Braman‡
University of Kansas, Lawrence, Kansas

A flight-test technique has been developed under NASA Dryden sponsorship to define the aerodynamic effect of thrust level on aircraft lift and drag characteristics. Conventional stabilized "speed power" tests require the thrust to be adjusted for each test condition and, as a result, the effect of thrust on aerodynamic characteristics cannot be easily identified. The technique utilizes quasi-steady-state maneuvers at selected power settings throughout the Mach range of the aircraft to define lift and drag coefficient variation as a function of angle of attack, Mach number, and power setting. A 20-h verification flight-test program was accomplished using a Learjet Model 35 aircraft. Significant power effects were identified which should be anticipated on any aircraft with jet engines mounted on the aft fuselage above the inboard wing section.

Nomenclature

a_x, a_z = acceleration along x and z wind axes, respectively
C_D = drag coefficient
C_{D_S} = drag coefficient corrected for skin-friction [Eq. (7)]
C_L = lift coefficient
C_{L_S} = lift coefficient corrected for thrust moment effect and nonstandard center of gravity [Eq. (4)]
C_{L_T} = lift coefficient corrected for thrust moment effect
C_f = skin-friction coefficient
F_g = gross thrust
F_r = ram drag
F_x, F_z = forces along x, and z wind axes, respectively
g = acceleration of gravity
L = lift
M = Mach number
m = aircraft mass
N_1 = low-pressure fan rpm
n_x, n_z = x and z wind axes load factors, respectively
P_a = ambient pressure
q = dynamic pressure
R_e = Reynolds number
S = wing reference area
W = aircraft weight
W_a, W_f = air and fuel flows, respectively
x,z = longitudinal and normal axes, respectively
α = angle of attack
δ = pressure ratio
γ = flight-path angle
γ' = ratio of specific heat for air
λ = thrust inclination angle
ρ = air density

Introduction

IN-FLIGHT definition of the aerodynamic effect of thrust level on lift and drag characteristics has not been possible in the past. Normally lift and drag measurements are accomplished using a series of stabilized points throughout the aircraft flight envelope. A wide range of engine power settings is used to achieve the stabilized conditions from which lift and drag may be determined given an in-flight thrust and airflow model along with normally instrumented aircraft parameters such as weight and angle of attack. Unfortunately, the flowfield around the aircraft may be altered significantly by the airflow through engine(s) which will result in the lift and drag characteristics being directly dependent on engine power. If the stabilizer point method is used on an aircraft where power effects are significant, use of the resulting data to predict nonstabilized (i.e., excess thrust not equal to zero) performance characteristics will be susceptible to significant error. A flight-test technique has been developed to efficiently evaluate the effect of engine power setting on the lift and drag characteristics of an aircraft. The technique utilized quasi-steady-state maneuvers (level accelerations and decelerations) at selected power settings throughout the Mach range of the aircraft to define lift and drag coefficient variation as a function of angle of attack, Mach number, and power setting. The technique was developed and evaluated during a 20-h flight-test program using a Learjet Model 35 aircraft. This effort was part of an overall research program which concentrated on modeling aircraft performance throughout the flight envelope. The use of quasi-steady-state maneuvers not only allowed definition of power effects on lift and drag, but also provided a very time-efficient approach to overall in-flight aircraft performance definition when compared to the stabilized point method.

Concept

Development of the lift and drag characteristics from quasi-steady-state maneuvers began with consideration of the forces acting on the aircraft. The aircraft force balance equations resolved parallel and perpendicular to the flight path (assuming zero sideslip, wings level, and constant mass) are, from Fig. 1,

$$\Sigma F_x = ma_x$$

$$F_g\cos(\alpha+\lambda) - F_r - D = W[(a_x/g) + \sin\gamma]$$

$$\Sigma F_z = ma_z$$

$$L + F_g\sin(\alpha+\lambda) = W[(a_z/g) + \cos\gamma]$$

Presented as Paper 84-0563 at the AIAA 22nd Aerospace Sciences Meeting, Reno, Nev., Jan. 9-12, 1984; received May 11, 1984; revision received Sept. 11, 1984.

*Lt. Col., USAF, Associate Professor. Member AIAA.
†Associate Professor. Associate Fellow AIAA.
‡Graduate Student. Member AIAA.

As discussed in Ref. 1, the flight-path load factors resolved along the x and z wind axes are

$$n_x = (a_x/g) + \sin\gamma, \qquad n_z = (a_z/g) + \cos\gamma$$

The force balance equations then may be expressed as

$$F_g\cos(\alpha+\lambda) - F_r - D = Wn_x$$

$$L + F_g\sin(\alpha+\lambda) = Wn_z$$

and the relationships for lift and drag coefficients are

$$C_L = \frac{Wn_z - F_g\sin(\alpha+\lambda)}{\tfrac{1}{2}\gamma' p_a M^2 S} \tag{1}$$

$$C_D = \frac{F_g\cos(\alpha+\lambda) - F_r - Wn_x}{\tfrac{1}{2}\gamma' p_a M^2 S} \tag{2}$$

Equations (1) and (2) express lift drag coefficients in terms of wind axis accelerations, the engine model parameters of gross thrust and ram drag, and normally recorded flight-test parameters such as angle of attack, ambient pressure, weight, and Mach number. The equations are compatible with quasi-steady-state maneuvers where excess thrust is not equal to zero and flight-path accelerations are present. Wind axis accelerations were determined from accelerometers mounted along the body axis of the aircraft using the appropriate angular transformations. A unique in-flight thrust and airflow prediction technique, termed "thrust modeling," was developed as part of the overall program to define the gross thrust and ram drag terms in Eqs. (1) and (2). The technique consisted of correcting the engine deck predictions of thrust and airflow to match the performance of the actual engines installed in the aircraft using a three-step approach:

1) Simplified representation of engine deck predicted thrust, fuel flow, and airflow in corrected form.

2) Correction of the engine deck model, developed in step 1, to the individual characteristics of each engine based on a static thrust run.

3) In-flight correction of thrust and airflow predictions based on actual test fuel flow, an accurate specific fuel consumption prediction, and a balance of the thrust momentum equation.

The final equations in simplified form for thrust and airflow were:

$$F_{g_{\text{test}}} = \frac{W_{f_{\text{test}}} F_{g_{\text{deck}}}}{\eta W_{f_{\text{deck}}}}$$

$$W_{a_{\text{test}}} = W_{f_{\text{test}}}\left[\frac{W_{a_{\text{deck}}}}{\eta W_{f_{\text{deck}}}} + \frac{1}{\eta} - 1\right]$$

where η is the ratio of static thrust run specific fuel consumption to engine deck specific fuel consumption defined as a function of corrected rpm. A complete development of this technique is presented in Ref. 2. Thrust and airflow prediction accuracies were believed to be 3-5% or better based on data obtained from the Lear 55, F-104G, F-111, and YF-12 programs.[2-5] This prediction technique offered several advantages over the most commonly used methods as discussed in Ref. 2.

Two corrections were made to lift coefficient for elevator trim effects resulting from 1) the thrust moment about the center of gravity (c.g.) and 2) a nonstandard c.g. These corrections standardized the lift coefficient data to a common baseline.

In the first case, the effect of the associated moments created by the thrust F_g and ram drag F_r about the c.g. were removed. From Fig. 2, this moment is given by

$$\Delta M_{\text{thrust}} = -F_g Z_{\text{thrust}} + F_r h_r$$

To counteract this moment, an incremental lift at the tail is needed, such that

$$-\Delta L_{\text{tail}}\ell_{\text{tail}} - F_g Z_{\text{thrust}} + F_r h_r = 0$$

and the change in lift coefficient which must be added to C_L is $-\Delta L_{\text{tail}}/\bar{q}S$ or

$$\Delta C_{L_{\text{thrust moment}}} = \frac{(F_g Z_{\text{thrust}} - F_r h_r)}{\ell_{\text{tail}} qS}$$

The trimmed lift coefficient C_{L_T} then becomes

$$C_{L_T} = C_L + \Delta C_{L_{\text{thrust moment}}}$$

The distance Z_{thrust} is a function of c.g. and airframe geometry, while h_r and ℓ_{tail} are also functions of angle of attack.

C_{L_T} was also standardized to a particular c.g. location. From Fig. 3, this correction begins with a moment balance

$$AL_{\text{wing}} = L_{\text{tail}}\ell_{\text{tail}} \quad \text{(test c.g.)}$$

$$L_{\text{wing}}(A - \Delta\text{c.g.}) = Z(L_{\text{tail}} + \Delta L_{\text{tail}}) \quad \text{(standard c.g.)}$$

where ΔL_{tail} is the change in tail lift required for a standard c.g.

Since

$$Z = \ell_{\text{tail}} + \Delta\text{c.g.}$$

$$L_{\text{tail}}\ell_{\text{tail}} - L_{\text{wing}}\Delta\text{c.g.} = (\ell_{\text{tail}} + \Delta\text{c.g.})L_{\text{tail}} + (\ell_{\text{tail}} + \Delta\text{c.g.})\ \Delta L_{\text{tail}} \tag{3}$$

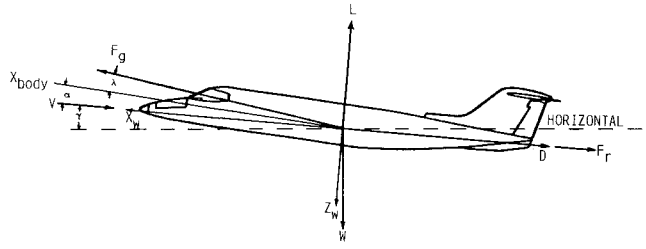

Fig. 1 Aircraft force balance diagram.

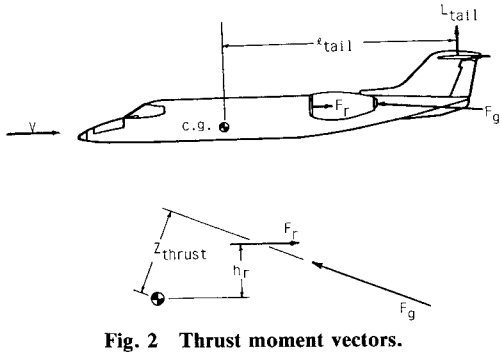

Fig. 2 Thrust moment vectors.

With the total aircraft lift L given by

$$L = L_{\text{wing}} + L_{\text{tail}}$$

for the test condition, Eq. (3) becomes

$$-L(\Delta\text{c.g.}) = (\ell_{\text{tail}} + \Delta\text{c.g.})\Delta L_{\text{tail}}$$

and

$$\Delta L_{\text{tail}} = \frac{-L(\Delta\text{c.g.})}{\ell_{\text{tail}} + \Delta\text{c.g.}}$$

In coefficient form,

$$\Delta C_{L_{\text{c.g.}}} = \frac{-C_{L_T}(\Delta\text{c.g.})}{(\ell_{\text{tail}} + \Delta\text{c.g.})}$$

and the standardized lift coefficient corrected for thrust moment effects and to a standard c.g. is

$$C_{L_S} = C_{L_T} + \Delta C_{L_{\text{c.g.}}} \tag{4}$$

A correction to the drag coefficient was made for skin-friction variation as a function of Reynolds number to standardize the drag coefficient data to a particular altitude. Schlichting's formula for the skin-friction coefficient assuming turbulent flow[6] was used.

$$C_f = \frac{0.455}{(\log_{10} R_e)^{2.58}(1 + 0.144M^2)^{0.65}} \tag{5}$$

where $R_e = \rho V\ell/\mu$; ℓ is the characteristic length and μ the viscosity coefficient.

The drag coefficient due to skin friction is then

$$C_{D_{\text{SF}}} = C_f\left(\frac{\text{wetted area}}{S}\right) \tag{6}$$

where the drag contribution of the aircraft components is broken down according to the following parameters: fuselage, wing, horizontal tail, vertical tail, engine pylons, engine nacelles, ventral fin, tip tanks, and tank fins.

The Reynolds number calculation of Eq. (5) requires the characteristic length and the applicable wetted area is needed to calculate $C_{D_{\text{SF}}}$ in Eq. (6). The skin-friction drag contributions then were standardized to an altitude of 25,000 ft by computing $C_{f_{25,000}}$, and $C_{D_{\text{SF}}}$ and defining the incremental change in drag coefficient due to skin-friction variation for off-standardized conditions as

$$\Delta C_{D_{\text{SF}}} = C_{D_{\text{SF}_{25,000\text{ ft}}}} - C_{D_{\text{SF}}}$$

This methodology was used for each of the aircraft components and the total skin friction drag correction $\Delta C_{D_{\text{SF}}}$ was obtained by summing the contribution of each component.

$$\Delta C_{D_{\text{SF}_{\text{total}}}} = \Delta C_{D_{\text{SF}_{\text{fuselage}}}} + \Delta C_{D_{\text{SF}_{\text{wing}}}} + \Delta C_{D_{\text{SF}_{\text{horizontal tail}}}}$$
$$+ \Delta C_{D_{\text{SF}_{\text{vertical tail}}}} + \Delta C_{D_{\text{SF}_{\text{pylon}}}} + \Delta C_{D_{\text{SF}_{\text{nacelles}}}}$$
$$+ \Delta C_{D_{\text{SF}_{\text{ventral fin}}}} + \Delta C_{D_{\text{SF}_{\text{tank}}}} + \Delta C_{D_{\text{SF}_{\text{tank fin}}}}$$

The standardized drag coefficient C_{D_S} is then

$$C_{D_S} = C_D + \Delta C_{D_{\text{SF}_{\text{total}}}} \tag{7}$$

An altitude of 25,000 ft was chosen for standardization, since it was approximately in the middle of the altitude envelope of the aircraft.

C_{L_S} and C_{D_S} vs angle-of-attack characteristics were defined from a series of test points obtained during acceleration/deceleration maneuvers. These characteristics were defined as a function of power setting and Mach number. The needed lift coefficient range was obtained through variation of the weight-pressure ratio (W/δ) as discussed in the following section. By determining the lift and drag characteristics as a function of power setting, the power-dependent effects could be defined when comparing data for the same Mach number and angle of attack.

Test Procedure

Quasi-steady-state acceleration/deceleration maneuvers provided the necessary data to define lift and drag characteristics. These maneuvers were conducted at nearly constant altitude using the altitude hold mode of the autopilot. Normally less than a 60-ft excursion from the start altitude was experienced during a maneuver. Eight "cardinal"

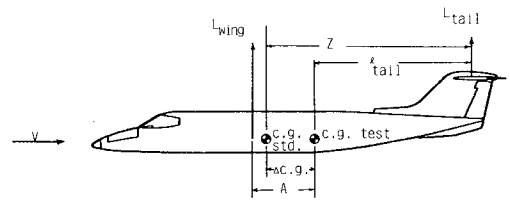

Fig. 3 Moment arms for c.g. standardization.

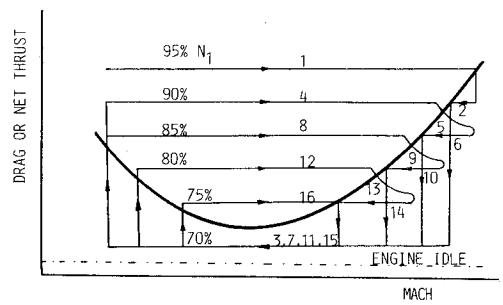

Fig. 4 Typical maneuvering sequence.

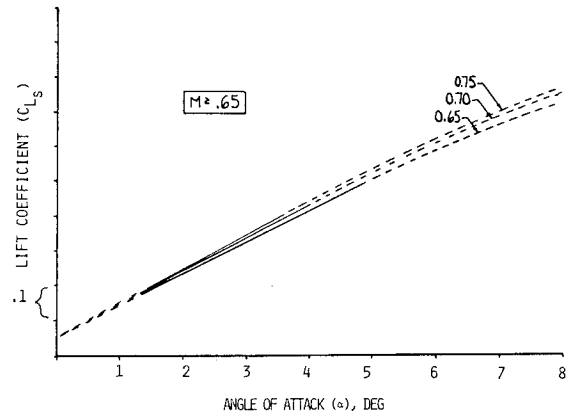

Fig. 5 Lift coefficient characteristics, $M \geq 0.65$.

power settings were evaluated consisting of 95, 90, 85, 80, 75, 70, 60, and 50% N_1. The N_1 was chosen as the variable to represent power because of the relatively high bypass ratio of the engines and the resulting high correlation to engine airflow. An acceleration/deceleration was conducted at a cardinal power setting by holding N_1 to within ±0.5% during a maneuver. A range of the weight-pressure ratio parameter (W/δ) within the aircraft envelope was designated to provide a lift coefficient variation for a given Mach number so that Mach effects could be defined. Eight values of W/δ were evaluated as shown in Table 1. These eight values of W/δ provided eight evenly spaced points on a constant Mach drag polar in the mid-Mach range. At each value of W/δ, an acceleration/deceleration sequence was performed which included maneuvers at all cardinal power settings above idle. As W/δ increased, the number of available power settings decreased because the idle rpm increases with altitude. For example, at 40,000 ft only the 95, 90, and 85% power settings could be evaluated. As a result, the largest amount of data was obtained for the higher power settings.

A typical maneuvering sequence is illustrated in Fig. 4 which assumes the drag curve and engine idle level are as shown for a particular W/δ configuration. A sequence began by slowing the aircraft to an acceptable minimum speed (for the Lear 35 this was an airspeed slightly above stick shaker speed) at an altitude based on the target value of W/δ. A 95% acceleration then was performed. When the acceleration had slowed to approximately 0.25 knot/s, the throttles were retarded to 90% and a deceleration performed until a stabilized point was approached. The sequence then continued as shown in Fig. 4 and Table 2. Altitude adjustments were made at convenient times in the sequence to maintain W/δ within approximately ±1% as weight decreased. Although not specifically shown in Fig. 4, a high-power setting for sequence 9 was used to accelerate past the last stabilized condition so that the deceleration as shown in sequence 10 could be obtained (Table 2). Although a stabilized "speed power" point was generally not obtained, the Mach number for which the drag and net thrust curves intersected could easily be estimated based on the Mach region where the acceleration and deceleration for a particular power setting were terminated. The general guideline used was to accelerate far enough past the last stabilized condition so that the engine rpm would achieve stabilization on the subsequent deceleration before reaching the Mach number of the last stabilized point. Data were taken periodically throughout an acceleration/deceleration rather than continually to keep the volume of data to a manageable level. Ideally, approximately a 20-s burst of data was recorded as the aircraft passed through each 0.05 Mach increment. The actual test sequence peformed at each W/δ condition depended directly on the location of the drag curve with respect to the net thrust levels. For example, if two cardinal power settings were located between engine idle and the bottom of the drag curve, then at least one deceleration would be performed at each of these power settings. The maneuver sequence was designed to acquire the needed data in a time-efficient manner and also be easily accomplished by the flight crew. It clearly met these objectives. For planning purposes, approximately 45 min were required to accomplish a maneuvering sequence at one value of W/δ for this aircraft.

Table 1 Performance modeling maneuvering sequences

W/δ	Nominal altitude, ft
22,000	10,000
40,000	23,000
47,000	26,000
53,000	29,000
60,000	32,000
67,000	35,000
73,000	38,000
80,000	40,000

Table 2 Maneuvering sequence description

Sequence	Power setting	Maneuver	Data recorded
1	95	Accel	Yes
2	90	Decel	Yes
3	70	Decel	Yes
4	90	Accel	Yes
5	95	Accel	No
6	85	Decel	Yes
7	70	Decel	Yes
8	85	Accel	Yes
9	95	Accel	No
10	80	Decel	Yes
11	70	Decel	Yes
12	80	Accel	Yes
13	95	Accel	No
14	75	Decel	Yes
15	70	Decel	Yes
16	75	Accel	Yes

Results

The C_{L_S} vs angle-of-attack characteristics for the Lear 35 fell into two distinct categories. Above 0.65 Mach, power effects were negligible; but distinct Mach effects were identified. A summary of the standardized lift coefficient characteristics in this high Mach region is presented in Fig. 5, where an increase in Mach number resulted in an increase in C_{L_S} as well as the slope C_{L_α}. The extrapolated portions of each curve are identified by the uniform dashed lines as indicated. Below 0.65, Mach effects were negligible, but power effects were found as presented in Fig. 6. At power settings above 60%, a small but significant increase in C_{L_S} was observed. At 70% power, approximately a 0.01 increase in C_{L_S} resulted throughout the angle-of-attack range when compared to the data from the 60% power curve. As power was increased to 75% and above, an additional increase of approximately 0.01 over the 70% curve was found. The data scatter experienced when defining the C_{L_S} vs α curves presented in Figs. 5 and 6 was ±0.02 maximum (based on C_{L_S} with approximately 95% of the data falling within ±0.01 of the defined curves.

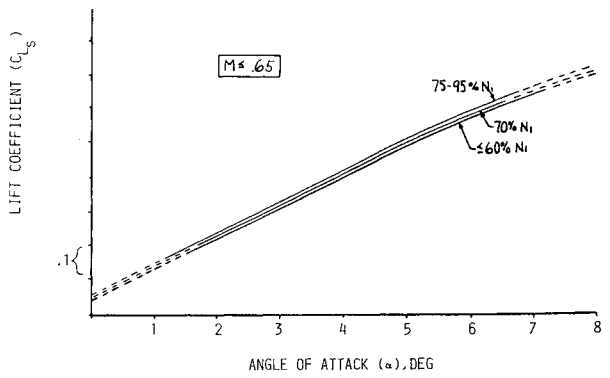

Fig. 6 Lift coefficient characteristics, $M \leq 0.65$.

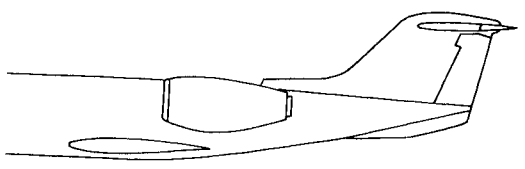

Fig. 7 Engine/airframe configuration.

The power effects on C_{L_S} are thought to be directly related to the close approximity of the engine inlets above the inboard upper wing surface as profiled in Fig. 7. Either of two effects could be present. First, the flowfield around the wing/nacelle may be fairly normal at high engine speed, however, at low engine speed, inlet spillage reduces the lift over the inboard section of the wing by retarding the flow. Second, above 60% power, the increased airflow through the engine may alter the flowfield in the engine nacelle/wing root area such that the overall circulation around the inboard wing section is increased, resulting in a corresponding increase in lift. This increase in lift does not continue with increasing power settings above 75% but rather remains constant at approximately the 75% value. The increased airflow through the engine with increasing power may produce an increase in lift on the forward portion of the inner wing but may also result in flow starvation and separation near the trailing edge, producing an offsetting effect. Obviously, a flowfield survey in the engine nacelle/wing root area is needed to help explain these power effects. Flow tufting in this area would be an excellent first step in understanding the power effects observed and could easily be accomplished concurrently with the quasi-steady-state maneuvers used for performance modeling.

As with lift coefficient, C_{D_S} vs angle-of-attack characteristics fell into two distinct and consistent categories. For 0.6 Mach and above, power effects were not observed but Mach effects were identified. A summary of the standardized drag coefficient characteristics in the high Mach region is presented in Fig. 8 where an increase in Mach number generally resulted in an increase in C_{D_S} for a given angle of attack. As shown in Fig. 8, the largest increase in C_{D_S} with Mach number was projected above 4-deg angle of attack. For 0.55 Mach and below, Mach effects were not significant but power effects were found. As presented in Figs. 9 and 10, C_{D_S} generally decreased as power decreased with approximately a 45 drag count band between 90 and 50% power in the mid-angle-of-attack region. The 95% power curve intersected and crossed over the 90% curve at two locations and dropped below the 90% curve in the mid-angle-of-attack region as shown. The data scatter experienced when defining the C_{D_S} vs α curves presented in Figs. 8-10 was ± 0.003 maximum (based on C_{D_S}) with approximately 95% of the data falling within ± 0.001 of the defined curves.

As with the lift coefficient curves, the complex flow interaction in the nacelle/wing root area must be analyzed to understand these characteristics. Normally it would be expected that lower drag would occur at higher power settings due to reduced inlet spillage. This trend is seen in the mid-angle-of-attack region for 90 and 95% power (Fig. 9). Obviously, however, this is not the only factor to affect the drag. Another possible interaction may be an increased pressure on the aft-facing wing and fuselage surfaces (a drag reduction) resulting from increased inlet spillage at the lower power settings. The close proximity of the engine nacelle to these surfaces makes this occurrence quite feasible. In Fig. 9, the crossover experienced by the 95% curve in the higher angle-of-attack region (lower speed) indicates that the increased pressure phenomenon may become predominant as the aft-facing wing and fuselage surfaces increase with angle of attack and as propagation of the inlet spillage air also increases with lower speed. Another contributing factor may be increased flow starvation and separation near the wings trailing edge with increasing power, as discussed in the section on lift. This would account for the increased drag observed with increased power. The absence of power effects on drag at 0.6 Mach and above is probably due to the low propagation of inlet spillage air at higher speeds. Again, a flowfield survey in the wing root/nacelle area would help clarify the causes of the identified drag characteristics.

A selected number of steady-state (speed power) points were flown for comparison. Excellent agreement was obtained between the steady-state points and the curves presented in Figs. 5-10. The maximum deviation for C_{L_S} was 0.01 and for C_{D_S} was 0.001 which was clearly within the observed data scatter. The maximum magnitudes of the thrust moment, c.g., and skin-friction corrections were also determined for the flight-test conditions evaluated. The maximum values for $\Delta C_{L_{\text{thrust moment}}}$, $\Delta C_{L_{c.g.}}$, and $\Delta C_{D_{SF}}$ were 0.003, 0.005, and 0.0012, respectively, which indicate that these corrections had a relatively small but still significant effect on the data.

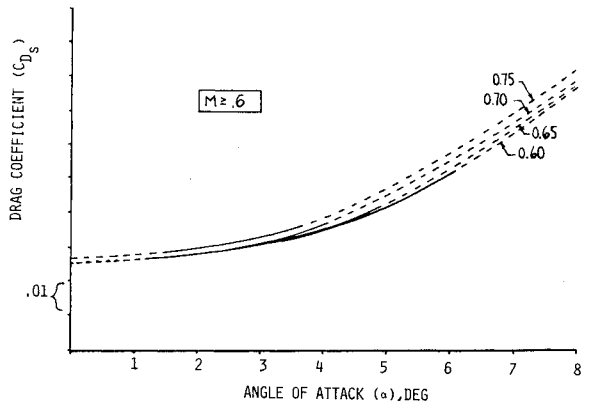

Fig. 8 Drag coefficient characteristics, $M \geq 0.6$.

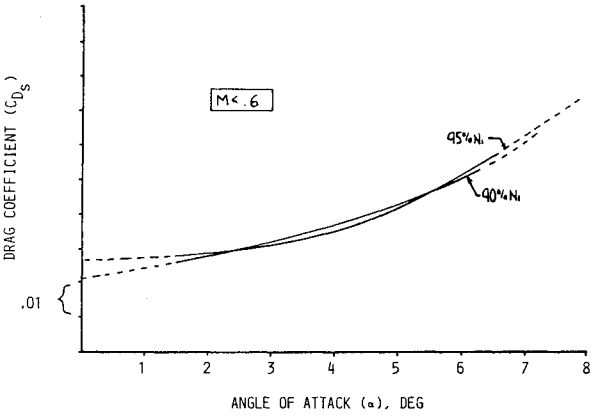

Fig. 9 Drag coefficient characteristics, $M \leq 0.55$, 90 and 95% N_1.

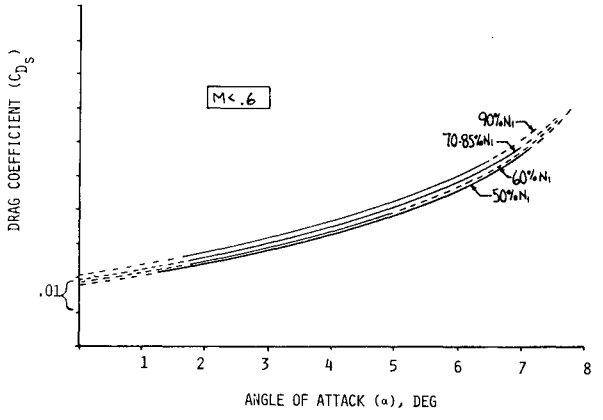

Fig. 10 Drag coefficient characteristics, $M \leq 0.55$, 50-90% N_1.

Conclusions

A in-flight technique was developed to define the aerodynamic effect of thrust level (power effects) on aircraft lift and drag characteristics. A time-efficient test approach was used which relied primarily on level acceleration and deceleration maneuvers. Flight-test results for the Learjet Model 35 aircraft showed that power effects were very signifi-

cant and must be considered if the data is to be used for predictions of aircraft performance under nonsteady flight conditions. It was believed that the power effects found on the Lear 35 were directly related to the complex flowfield in the wing root area resulting from the overwing mounting of the engines. In general, the approach developed in this program should be applicable to a large range of both jet- and propeller-powered aircraft.

References

[1]Simpson, W. R., "The Accelerometer Methods of Obtaining Aircraft Performance from Flight Test Data," Center for Naval Analysis, Alexandria, Va., Professional Paper 245, June 1979.

[2]Braman, K. B., Schweikhard, W. G., and Yechout, T. R., "Thrust Modeling, A Simplified Thrust and Airflow Prediction Technique for Flight Test Performance Measurements," AIAA Paper 83-2751, Nov. 1983.

[3]Marshal, R. T. and Schweikhard, W. G., "Modeling of Aircraft Performance from Flight Test Results and Validation with an F-104G Airplane," NASA TN D-7137, 1973.

[4]Redin, P. C., "Application of a Performance Modeling Technique to an Airplane with Variable Sweep Wings," NASA TP 1855, 1981.

[5]Redin, P. C., "A Performance Model of the YF-12C Airplane," YF-12 Experiments Symposium, NAA CP-2054, Vol. 3, 1978, pp. 409-534.

[6]Schlichting, H., "Turbulent Boundary Layers at Zero Pressure Gradient," *Boundary Layer Theory*, 7th ed., McGraw-Hill Book Co., New York, 1979, pp. 635-665.